Elliptical distortion of the Milky Way's rotation traced by high-mass star-forming regions

Ping-Jie Ding[1,2], Zi Zhu[1,2] and Jia-Cheng Liu[1,2]

[1] School of Astronomy and Space Science, Nanjing University, Nanjing 210023, China
[2] Key Laboratory of Modern Astronomy and Astrophysics (Nanjing University), Ministry of Education, Nanjing 210023, China

Received 2017 February 27; accepted 2017 August 16

Abstract The gravitational potential of the Milky Way is non-axisymmetric caused by a bar or triaxial halo, which dominates an elliptical rotation of the Milky Way. Employing a likelihood analysis, we exploit the astrometric data of the masers thoroughly and constrain the elliptical rotation of the Galaxy. The VLBA observed masers in high-mass star-forming regions are more distant tracers than stars observed in optical bandpass thus are more appropriate for studying the global feature of the Milky Way's rotation. A clear elliptical potential of the Milky Way is detected, with an ellipticity of $\epsilon_0 \sim 0.09$ at the Sun, and the ellipticity increases towards outer disk. The minor axis of the elliptical potential (the major axis of the rotation orbit) is found to be near the Sun with a displacement $\sim 32^\circ$. Based on the rotation model assumed for an elliptical potential, we also make a kinematical calibration of the Galactocentric distance of the Sun, which gives $R_0 = 7.63 \pm 0.34\,\mathrm{kpc}$.

Key words: astrometry — Galaxy: fundamental parameters — Galaxy: kinematics and dynamics — methods: data analysis

1 INTRODUCTION

The rotation feature of the Milky Way remains uncertain due to the limit of observations and the choice of models. The estimate of rotation speed at the location of the Sun varies from around $200\,\mathrm{km\,s^{-1}}$ to $\gtrsim 260\,\mathrm{km\,s^{-1}}$ (Elias et al. 2006; Zhu 2006; McMillan&Binney 2010; Reid et al. 2014; Sharma et al. 2014; Bobylev&Bajkova 2015b; Bobylev&Bajkova 2017) relying on different samples and methodologies. The rotation curve is found to be nearly flat in the solar neighborhood with a slight inclination (Uemura et al. 2000; Zhu 2006; López-Corredoira 2014; Huang et al. 2016) but the global feature of the rotation curve is still under debate (McMillan&Binney 2010; Chemin et al. 2015; Reid&Dame 2016). Traditionally the Milky Way's rotation is proposed to be circular. However, it has been found that some large-scale non-axisymmetric structures such as a bar in the central few kpc of the disk and a triaxial halo exist in the Galaxy (de Vaucouleurs 1970; Dwek et al. 1995; Rojas-Niño et al. 2015; Gerhard 2016), which can notably impact the shape of the Galactic rotation (Binney 1978; Blitz&Spergel 1991; Kuijken&Tremaine 1994; Kuijken 1996; Chemin et al. 2015). Under this circumstance a circular rotation model could be insufficient for describing the rotation of our home galaxy.

⋆ E-mail: zhuzi@nju.edu.cn

In the work of Kuijken&Tremaine (1994) (hereafter KT94), the authors formulated a non-axisymmetric model for describing the Milky Way's elliptical rotation and investigated the ellipticity of the rotation orbit using the data of HI gas, distant carbon stars, Cepheids, and HII regions. They pointed out that the Sun lies near the minor axis of the elliptical Galaxy's potential. Metzger et al. (1998) adopted 288 Cepheids to probe the non-axisymmetry of the disk based on the KT94 model and found the antisymmetric component of the rotation ellipticity to be $s_0 = 0.043 \pm 0.016$ near the Sun, together with an estimate of $R_0 = 7.66 \pm 0.32\,\mathrm{kpc}$ for the Galactocentric distance of the Sun. Moreover, using nearly 300 open clusters within a range of 3 kpc from the Sun, Zhu (2008) found a potential ellipticity $\epsilon_0 \sim 0.048 - 0.066$ and a displacement of the Sun from the minor axis of the potential around 30°. Some other research also suggests that the stellar kinematics in the solar neighborhood could reveal some non-axisymmetry in the Galactic rotation (Bovy et al. 2012; López-Corredoira et al. 2016).

The reliability of the measured Galactic parameters improve with both the spacial coverage of tracers and observation precision. The data of maser sources in high-mass star-forming regions (HMSFRs) are most appropriate for analyzing the non-axisymmetry in the Milky Way's rotation, since masers are young and bright sources widely spread over the disk (extending out to $> 8\,\mathrm{kpc}$ from the Sun). The Bar and Spiral Structure legacy (BeSSeL) Survey and the Japanese VLBI Exploration of Radio Astrometry (VERA) have yielded more than 100 astrometric measurements of maser sources associated with high-mass star-forming regions (HMSFRs). The typical accuracy of the measured parallaxes is $\sim 20\,\mu\mathrm{as}$ (Reid 2012). The first data release of the ongoing Gaia mission, by contrast, has announced a systematic error in parallaxes at a level of $\pm 0.3\,\mathrm{mas}$ (Lindegren et al., 2016), leading to a large uncertainty in the distance of stars far away from the Sun. Under this circumstance, the maser data provide the best sample for the research on the Milky Way's rotation in a large spacial coverage at this stage. In this work, we investigate the Galactic kinematics using the maser data given by Reid et al. (2014). Using the maximum-likelihood (ML) method presented in Aghajani&Lindegren (2013) (hereafter AL13), we develop a likelihood analysis to exploit data and analyze the elliptical Milky Way's rotation based on the KT94 model. We also make a kinematical calibration of the Galactocentric distance of the Sun.

Section 2 lays out the data sampling. In Section 3, we introduce the KT94 model and the likelihood analysis used in our work. Our results are given in Section 4. And we make discussion toward the results in Section 5.

2 DATA SAMPLE

The data used in our work are selected from 103 masers given in Table 1 of Reid et al. (2014), which consist of measurements of positions, parallaxes, proper motions, and line-of-sight velocities in the local standard of rest (LSR), v_{LSR}, associated with the observational uncertainties. The LSR is defined based on the standard solar motion $(U_\odot^{\mathrm{Std}}, V_\odot^{\mathrm{Std}}, W_\odot^{\mathrm{Std}}) = (10, 15, 7)\,\mathrm{km\,s^{-1}}$ (Reid et al., 2014) in the heliocentric Cartesian coordinate system such that u-axis points to the Galactic center (GC), v-axis to Galactic transverse rotation, and w-axis to the North Galactic Pole. The heliocentric line-of-sight velocity $\tilde{v}_r$ is recovered from v_{LSR}.

The criterion of data selection is based on the parallax errors. We reject sources with $\sigma_p/\tilde{p} \geq 0.1$ or $\sigma_p/\tilde{p}^2 \geq 0.5\,\mathrm{kpc}$. $\tilde{p}$ and σ_p are the observed parallax and the corresponding observational uncertainty. The second criterion is set to avoid a few sources with large distant uncertainties even their relative parallax errors < 0.1. We obtain a sample including 70 maser sources that meet the above criterion. Figure 1 shows the locations of the selected maser sources projected onto the Galactic plane. The main three spiral arms (i.e. Sagittarius, Local, and Perseus) are plotted in colours.

3 METHODOLOGY

In this section we introduce the analytic frame used to describe the Galactic kinematics. The stellar motions consist of two components: the rotation velocity following the rotation curve and the peculiar motion. We employ and generalize the ML method presented in AL13 to estimate the best-fitting Galactic parameters from the parallaxes, proper motions and heliocentric line-of-sight velocities of maser sources, taking into consideration the observational uncertainties.

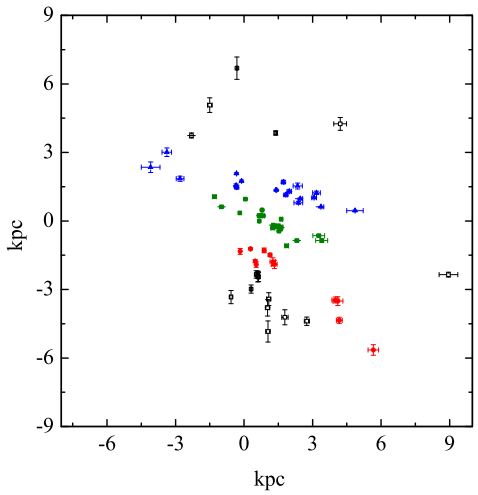

Fig. 1 Locations of the selected maser sources projected on the Galactic plane. The Sun is located at $(0,\ 0)$. The horizontal coordinate increases towards the direction of Galactic rotation and the vertical coordinate increases towards the Galactic anticenter. The red squares, olive circles, and blue triangles denote the sources resided in the Sagittarius, Local, and Perseus arms respectively. And the black squares denote the sources located in other regions.

In our analysis we introduce a Galactocentric cylindrical coordinate system $(R,\ \phi,\ z)$ such that R is the Galactocentric radius, z axis points to the North Galactic Pole from the GC and the azimuthal angle ϕ is measured in the direction of Galactic rotation.

3.1 Non-axisymmetric rotation model

The constraint on the shape of the rotation is based on the model described in KT94. The rotation curve is produced by a primarily axisymmetric potential coupled with a small non-axisymmetric potential. The total potential is written as:

$$\Psi(R,\ \phi) = \Psi_0(R) + \psi(R)\cos 2(\phi - \phi_b). \tag{1}$$

The axisymmetric part of the potential is power-law in Galactocentric radius proposed by KT94:

$$\Psi_0(R) = \begin{cases} \frac{V_0^2}{2\alpha}\left(\frac{R}{R_0}\right)^{2\alpha}, & \alpha \neq 0 \\ V_0^2 \ln(R), & \alpha = 0 \end{cases}, \tag{2}$$

where R_0 is the Galactocentric distance of the Sun and V_0 the circular speed at the solar position. The non-axisymmetric part of the potential in the KT94 model is also power-law dependent on radius:

$$\psi(R) = \psi_0 \left(\frac{R}{R_0}\right)^p,\ \psi_0 \geq 0. \tag{3}$$

The equipotential surfaces are approximately elliptical with axis ratio q. Setting $V_c(R)$ to be the circular velocity dominated by the axisymmetric part of the potential, the potential ellipticity ϵ is defined as $\epsilon(R) = 2\psi(R)/V_c(R)^2$, which is used to parameterize the non-axisymmetry of the rotation orbit. The relationship between ϵ and q is $\epsilon \backsimeq 1 - q$ to the first order. The parameter ϕ_b in Eq. (1) denotes the direction of the minor axis of the potential (i.e. the major axis of the orbit). The circular velocity and the

potential ellipticity at any radius R have the forms:

$$V_c(R) = V_0 \left(\frac{R}{R_0}\right)^{\alpha};\ \epsilon(R) = \epsilon_0 \left(\frac{R}{R_0}\right)^{p-2\alpha}, \tag{4}$$

and the rotation curve is given by

$$\begin{aligned} \bar{v}_R &= -\beta_1 V_c(R)\epsilon(R)\sin 2(\phi-\phi_b), \\ \bar{v}_\phi &= V_c(R) - \beta_2 V_c(R)\epsilon(R)\cos 2(\phi-\phi_b), \\ \bar{v}_z &= 0. \end{aligned} \tag{5}$$

The coefficients β_1 and β_2 are defined as

$$\beta_1 \equiv \frac{1+p/2}{1-\alpha},\ \beta_2 \equiv \frac{1+p(1+\alpha)/4}{1-\alpha}. \tag{6}$$

The KT94 model also gives the definitions of the two orthogonal terms of the ellipticity:

$$s_0 = \epsilon_0 \sin 2\phi_b,\ c_0 = \epsilon_0 \cos 2\phi_b, \tag{7}$$

which represent the antisymmetric and symmetric components of the ellipticity about the $\phi = 0^\circ$ line.

3.2 The maximum-likelihood (ML) estimation

The ML method formulated by AL13 is used for fully exploit the data when the observational uncertainties cannot be neglected. The authors of AL13 used the ML method to analyze the local kinematics when only parallaxes and proper motions are known. In this work we employ and generalize the AL13 method by introducing the measured line-of-sight velocities and the rotation curves. The observables include the parallax $\tilde{p}$, the proper motions in the directions of increasing Galactic coordinates l and b, i.e. $\tilde{\mu}_l$ and $\tilde{\mu}_b$, and the line-of-sight velocity $\tilde{v}_r$. Given the kinematical parameters $\boldsymbol{\theta} = (R_0,\ V_0,\ s_0,\ c_0,\ \boldsymbol{v}_\odot)$ (where $\boldsymbol{v}_\odot = (U_\odot,\ V_\odot,\ W_\odot)$ is the solar peculiar velocity), the velocity dispersion tensor $\boldsymbol{D}$, and the observables, the log-likelihood function of one source is

$$L(\boldsymbol{\theta}, \boldsymbol{D}, p) = \ln f_{\tilde{\boldsymbol{v}}}(\tilde{\boldsymbol{v}}|p) + \ln g(\tilde{p} - p), \tag{8}$$

where $f_{\tilde{\boldsymbol{v}}}$ is the probability density function (pdf) of the observed heliocentric velocity $\tilde{\boldsymbol{v}} = (k\tilde{\mu}_l/p,\ k\tilde{\mu}_b/p,\ \tilde{v}_r)$ when the true parallax p is known and g is the centered normal pdf with standard deviation σ_p. The constant $k = 4.74047$ if the units for the velocities, proper motions and parallaxes are $\mathrm{km\,s^{-1}}$, $\mathrm{mas\,yr^{-1}}$ and mas.

We now need an explicit expression for the conditional pdf $f_{\tilde{\boldsymbol{v}}}(\tilde{\boldsymbol{v}}|p)$. The expected value of $\tilde{\boldsymbol{v}}$, i.e. $\boldsymbol{v}$, is deduced from the rotation curve and $\boldsymbol{v}_\odot$ (see Appendix). The dispersion tensor is defined as $\boldsymbol{D} = \mathrm{diag}(\sigma_\mathrm{R}^2,\ \sigma_\phi^2,\ \sigma_\mathrm{z}^2)$, which parameterizes the effect of stellar peculiar motions relative to the expected motion modeled by the rotation curve. In this work we set $\sigma_R = \sigma_\phi = \sigma_z \equiv \Delta$ under the assumption that the random component of stellar velocities is isotropous and satisfies Gaussian distribution (McMillan&Binney, 2010). The total covariance of $\tilde{\boldsymbol{v}}$ is the sum of $\boldsymbol{D}_{\boldsymbol{v}}$ (the covariance due to the dispersion tensor, see Appendix) and the covariance due to the observational uncertainties:

$$\boldsymbol{C}_{\tilde{\boldsymbol{v}}} = \boldsymbol{D}_{\boldsymbol{v}} + \begin{pmatrix} k^2\sigma_{\mu_l}^2/p^2 & k^2\rho\sigma_{\mu_l}\sigma_{\mu_b}/p^2 & 0 \\ k^2\rho\sigma_{\mu_l}\sigma_{\mu_b}/p^2 & k^2\sigma_{\mu_b}^2/p^2 & 0 \\ 0 & 0 & \sigma_{v_r}^2 \end{pmatrix}, \tag{9}$$

where σ_{μ_l}, σ_{μ_b}, and σ_{v_r} are the observational uncertainties in μ_l, μ_b, and v_r respectively, and ρ the correlation coefficient between μ_l and μ_b. For the simplest case both the distribution of velocity dispersion and the observational errors are Gaussian. Thus the expression of $f_{\tilde{\boldsymbol{v}}}(\tilde{\boldsymbol{v}}|p)$ can be written as

$$f_{\tilde{\boldsymbol{v}}}(\tilde{\boldsymbol{v}}|p) = (2\pi)^{-\frac{3}{2}} |\boldsymbol{C}_{\tilde{\boldsymbol{v}}}|^{-\frac{1}{2}} \exp\left[-\frac{1}{2}(\tilde{\boldsymbol{v}} - \boldsymbol{v})^T \boldsymbol{C}_{\tilde{\boldsymbol{v}}}^{-1} (\tilde{\boldsymbol{v}} - \boldsymbol{v})\right]. \tag{10}$$

Table 1 Kinematical parameters describing the elliptical rotation based on the KT94 model with $\alpha = -0.1$, $\alpha = 0$, and $\alpha = 0.1$ respectively. The Galactocentric distance of the Sun is assumed to be $8.33\,\mathrm{kpc}$.

α	p	V_0 $(\mathrm{km\,s^{-1}})$	s_0 $(\times10^{-2})$	c_0 $(\times10^{-2})$	Δ $(\mathrm{km\,s^{-1}})$	ϵ_0 $(\times10^{-2})$	ϕ_b $(^\circ)$
-0.1	-1.73 ± 0.21	259.1 ± 5.8	10.5 ± 1.4	5.6 ± 1.9	9.23 ± 0.51	11.9	30.9
0	0.14 ± 0.19	235.0 ± 6.7	8.8 ± 1.7	2.5 ± 1.8	10.11 ± 0.65	9.1	37.1
0.1	0.66 ± 0.18	220.1 ± 7.9	9.2 ± 2.1	6.2 ± 2.0	9.70 ± 0.40	11.1	27.9

Now we return to Eq. (8) to solve the kinematical parameters with the ML method. The log-likelihood function L depends on both the kinematical parameters and the parallax p. We use the approximate solution formulated by AL13 to eliminate p in Eq. (8), and the expression of the likelihood function is simplified as

$$L(\boldsymbol{\theta}, \boldsymbol{D}) \simeq \ln f_{\tilde{\boldsymbol{v}}}(\tilde{\boldsymbol{v}}|\tilde{p}) + \frac{1}{2}\sigma_p^2 F^2(\tilde{p}), \tag{11}$$

where $F(\tilde{p}) = (\partial \ln f_{\tilde{\boldsymbol{v}}}(\tilde{\boldsymbol{v}}|p)/\partial p)_{p=\tilde{p}}$. This is the log-likelihood expression for one source and the total log-likelihood function used for all the sources should be written as

$$L(\boldsymbol{\theta}, \boldsymbol{D}) \simeq \sum_{i=1}^{N} \left[f_{\tilde{\boldsymbol{v}},i}(\tilde{\boldsymbol{v}}_i|\boldsymbol{\theta}, \boldsymbol{D}, \tilde{p}_i) + \frac{1}{2}\sigma_{p,i}^2 F_i^2(\tilde{p}_i) \right]. \tag{12}$$

4 RESULTS

Since most sources are distributed in the azimuthal range of $-20^\circ < \phi < 60^\circ$, the solar peculiar velocity $\boldsymbol{v}_\odot$ has a non-negligible impact on constraining the rotation shape. Thus we fix the values for $\boldsymbol{v}_\odot$ whose components are $(11.1,\ 12.24,\ 7.25)\,\mathrm{km\,s^{-1}}$ (Schönrich et al., 2010).

Since we focus on the elliptical distortion in the Milky Way's rotation, the value of α in the KT94 model should be fixed in our analysis. The radial gradient of the rotation speed has been found nearly zero in the solar neighborhood (Zhu 2008, Bovy et al. 2012, Reid et al. 2014). In this case we choose $\alpha = 0$ to constrain the two-dimensional rotation and analyze the stellar motions.

4.1 Non-axisymmetric rotation curve based on the KT94 model

In the first place, the value of R_0 is fixed to be $8.33\,\mathrm{kpc}$ (Gillessen et al. 2009), which was derived from the stellar orbits around the massive black hole in the center of the Milky Way. We employ a Markov Chain Monte Carlo method (Metropolis et al., 1953, MCMC) to determine the best-fitting parameters for the KT94 model from the likelihood function in Eq. (12).

The estimated parameters are listed in Table 1, where we also give the results in the cases of $\alpha = -0.1$ and $\alpha = 0.1$ as a comparison. The results of ϵ_0 and ϕ_b are deduced from s_0 and c_0. The orbit ellipticity at $R = R_0$, ϵ_0, is significant for all the cases with a value $\gtrsim 0.09$. The azimuth of the minor axis of the elliptical potential (the major axis of the orbit) is at a level of 30°.

In the work of Metzger et al. (1998), the authors exploited the data of Cepheids and investigated the asymmetric component of ellipticity s_0, by fixing the symmetric ellipticity $c_0 = 0$. They found $s_0 \sim 0.004 - 0.071$, relying on the varying p and α. And the corresponding V_0 changes from around $197\,\mathrm{km\,s^{-1}}$ to around $293\,\mathrm{km\,s^{-1}}$. Fixing $c_0 = 0$ led to systematic bias in the final results, and it is beyond doubt that the determined period-luminosity relation introduced additional uncertainties to the derived kinematical parameters. As for the open cluster, which is another kind of good tracers for the Milky Way's rotation shape, Zhu (2008) divided the sample into different age ranges and estimated the values of ϵ_0 and ϕ_b. For the open clusters younger than 50 Myr, the estimated parameters are

$\epsilon_0 = 0.054 \pm 0.013$ and $\phi_b = 29.5^\circ \pm 3.3^\circ$, while the behaviour of older open clusters suggests a slightly smaller ellipticity $\epsilon_0 = 0.047 \pm 0.023$ and a major axis (of the orbit) slightly closer to the Sun, i.e. $\phi_b = 27.7^\circ \pm 7.7^\circ$. Since the measured Cepheids and open clusters are mostly confined to the solar neighborhood, the model parameters describing the elliptical rotation, namely (p, V_0, s_0, c_0) or (p, V_0, ϵ_0, ϕ_b) were difficult to constrain at the same time. Sampling the maser sources, we can obtain the estimates of p, V_0, s_0, c_0 simultaneously. The rotation ellipticity traced by masers is ~ 0.04 larger than that traced by Cepheids or open clusters. Nonetheless, the major axis of the orbit is verified close to the Sun, which indicates that stars in the solar vicinity are moving outward to the apocentre. The R- and ϕ-direction rotation velocities at the location of the Sun are around $22\,\mathrm{km\,s^{-1}}$ and $229\,\mathrm{km\,s^{-1}}$ respectively in the case of $\alpha = 0$. The left panel of Fig. 3 presents the residual map based on the $\alpha = 0$ model. And the radial and azimuthal residual velocities are shown in the left panel of Fig. 4 as functions of R.

Table 2 gives the correlation coefficients between the estimated parameters in the $\alpha = 0$ model, which tells us that the correlation between V_0 and c_0 is the most strong. The degeneracy between V_0 and c_0 is clearly shown in Fig. 2, which is attributed to the limited azimuthal coverage of data. More tracers at different azimuths and radii will break the degeneracy between parameters.

Table 2 Correlation coefficients between parameters in the KT94 model in the case of $\alpha = 0$.

	p	V_0	s_0	c_0	Δ
p	1	-0.33	-0.03	-0.08	$+0.09$
V_0		1	-0.37	-0.44	$+0.02$
s_0			1	$+0.18$	-0.07
c_0				1	$+0.00$
Δ					1

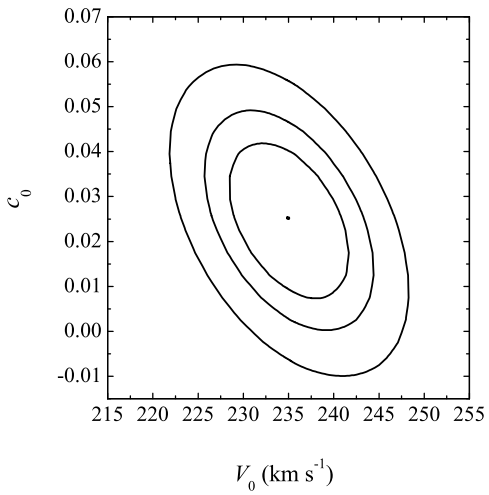

Fig. 2 Contours of the log-likelihood function projected in the (V_0, c_0)-plane for the KT94 model in the case of $\alpha = 0$. Contours are drawn at log-likelihood constants differing from the maximum $\Delta L = 0.5,\ 1,\ 2$, respectively.

Table 3 Galactic parameters calibrated by the KT94 model.

α	p	R_0 (kpc)	V_0 ($\mathrm{km\,s^{-1}}$)	s_0 ($\times10^{-2}$)	c_0 ($\times10^{-2}$)	Δ ($\mathrm{km\,s^{-1}}$)	ϵ_0 ($\times10^{-2}$)	ϕ_b ($^\circ$)
-0.1	-2.33	7.64 ± 0.37	242 ± 12	7.7 ± 1.4	5.1 ± 1.6	9.60 ± 0.66	9.2	28.1
0	0.20	7.63 ± 0.34	215 ± 10	8.1 ± 2.0	3.9 ± 2.0	9.81 ± 0.69	9.0	32.1
0.1	0.96	7.13 ± 0.33	192.2 ± 8.8	4.8 ± 1.6	6.4 ± 1.2	9.96 ± 0.67	8.0	18.3

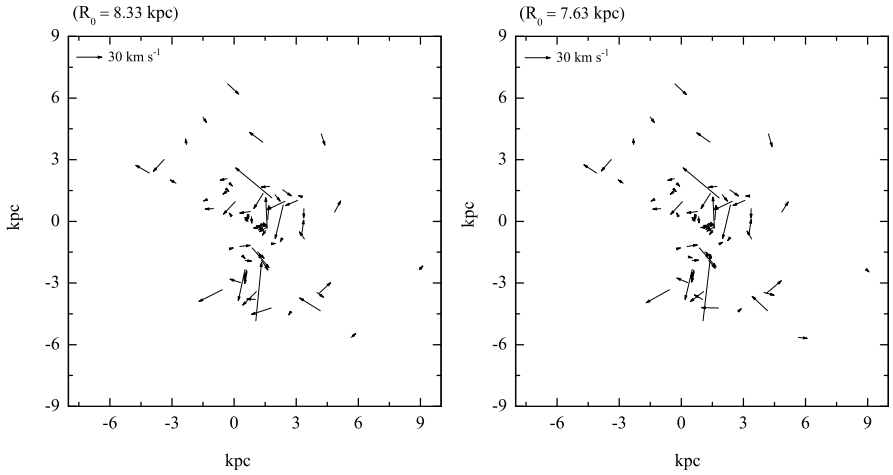

Fig. 3 Residual velocities of the 70 maser sources projected on the Galactic plane for the KT94 model in the case of $\alpha = 0$. The Sun is located at $(0,\, 0)$. The horizontal coordinate increases towards the direction of Galactic rotation and the vertical coordinate increases towards the Galactic anticenter. The left panel is based on the parameters constrained in the case of $R_0 = 8.33\,\mathrm{kpc}$ (see the second row of Table 1); the right panel is based on the parameters when R_0 is derived as $7.63\,\mathrm{kpc}$ using an iteration method (see the second row of Table 3).

4.2 Kinematical calibration of R_0

In the above analysis, we fixed the Galactocentric distance to be $R_0 = 8.33\,\mathrm{kpc}$. It is noteworthy that the value of R_0 is still debatable. On the one hand, measuring the trigonometric parallax of Sgr B2, a massive star-forming region in the GC, Reid et al. (2009) reported an estimate of $7.9^{+0.8}_{-0.7}$ kpc. On the other hand, fitting kinematic data of sampled tracers to a chosen rotation model, the constraint of R_0 varies from around 7 kpc to nearly 9 kpc (Shen&Zhu 2016, Gillessen et al. 2009, McMillan&Binney 2010, Schönrich 2012, Bobylev 2013, Matsunaga et al. 2013, Reid et al. 2014, Pietrukowicz et al. 2015, Boehle et al. 2016). In most cases, the kinematical ways of constraining R_0 were based on an assumption that the Milky Way's rotation is circular. In this work, considering the globally non-axisymmetric nature of the Galactic disk, we make a kinematical calibration of R_0 using an iteration method, given a prior for the model parameter p. Fixing the parameter p obtained by adopting an initial value of R_0 (see Table 1), we determine a new estimate of R_0. Then using the new R_0 as a fixed parameter, a new estimate of p can be derived. The iteration is repeated until convergence is achieved. For each case ($\alpha = -0.1$, $\alpha = 0$, or $\alpha = 0.1$), we have changed the initial value of R_0 from 6.7 to 8.9 kpc (McMillan&Binney, 2010) and found all these initial values converge to the consistent final solution. The final results are listed in Table 3. The residual map derived from the parameters in the case of $\alpha = 0$ is presented in the right panel of Fig. 3. And the radial and azimuthal residual velocities along with R (deduced from the new estimate of R_0) are plotted in the right panel of Fig. 4.

Table 4 Best-fitting parameters derived from sources resided in the Sagittarius (Sgr) arm, the Local (Loc) arm, and the Perseus (Per) arm respectively in the case of $\alpha = 0$, $p = 0.2$. The value of R_0 is adopted as $7.63\,\mathrm{kpc}$.

Spiral arm	V_0 $(\mathrm{km\,s^{-1}})$	s_0 $(\times 10^{-2})$	c_0 $(\times 10^{-2})$	Δ $(\mathrm{km\,s^{-1}})$	ϵ_0 $(\times 10^{-2})$	ϕ_b $(^\circ)$
Sgr	212.8 ± 8.4	4.3 ± 2.2	5.1 ± 2.0	7.2 ± 1.7	6.7	20.1
Loc	197.7 ± 9.3	8.5 ± 2.2	3.4 ± 2.2	7.61 ± 0.96	9.2	34.2
Per	230 ± 14	7.4 ± 2.4	3.8 ± 2.2	13.4 ± 1.6	8.3	31.4

Our results for R_0 yielded using the KT94 model is basically coincident with the estimates in Metzger et al. (1998), which gave $R_0 \sim 7.45 - 7.83\,\mathrm{kpc}$. Generally, in order to availably constrain R_0 on the basis of a rotation model, we need astrometric data of bright young objects such as masers, OB-type stars, open clusters, classical Cepheids, etc., which are located near the Galactic plane and have small dispersions in the velocity field. It is well-known that new-born stars in the cold disk are generally resided in the spiral arm, which means that the spiral structure could deviate the regional rotation orbit of these stars. Nonetheless, the elliptical rotation of the Milky Way is thought to be caused by the central bar's or the triaxial halo's influence, thus all the objects that feel the same gravitational potential cannot avoid being affected by the non-axisymmetry of the Galaxy's potential. In our estimation for R_0, we focus on the global rotation of the disk and assume that all the sampled tracers rotate around the GC in the potential formulated by KT94. In this case, the value of R_0 can be constrained tightly thanks to the widely distributed maser tracers.

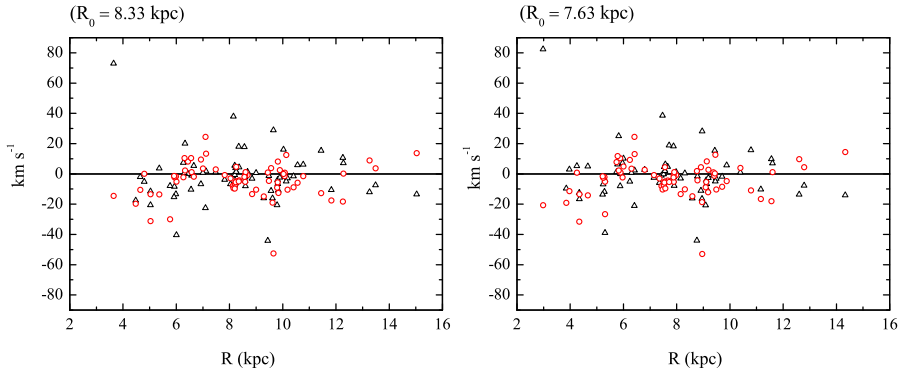

Fig. 4 Radial (black trangles) and azimuthal (red circles) residual velocities versus R for the KT94 model in the case of $\alpha = 0$. The left panel is based on the parameters constrained in the case of $R_0 = 8.33\,\mathrm{kpc}$ (see the second row of Table 1); the right panel is based on the parameters when R_0 is derived as $7.63\,\mathrm{kpc}$ using an iteration method (see the second row of Table 3).

5 DISCUSSION

The prolate or triaxial structures in the Galaxy (e.g. the bar, bulge, and triaxial halo) could dominate the distortion of the Galaxy's potential. Introducing a first-order non-axisymmetric rotation model, we have reconstructed the rotation curve of the Milky Way and calibrated the Galactocentric distance of the Sun.

In our analysis, we focus on the global kinematical feature of the Milky Way. It is noteworthy that the spiral structure could also introduce some bias in the rotation since stars participate in both the global rotation of the Milky Way and the specific motion of the arm in which they resided. In order to compare the kinematics of different arms, we select 12, 23, and 18 sources from the Sagittarius, Local, and Perseus arms and explore their rotations respectively. We assume $\alpha = 0$ for each of the arms. The

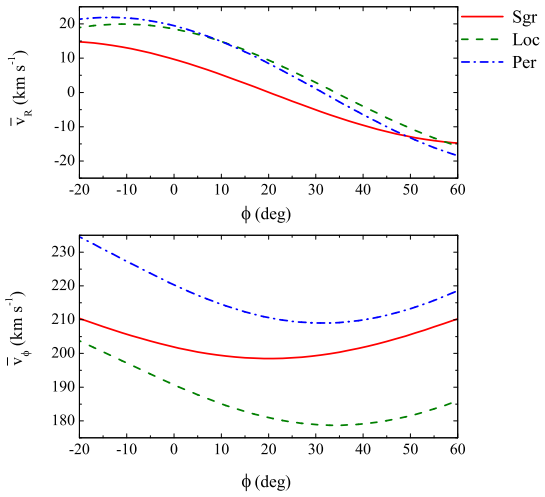

Fig. 5 Model velocities along the azimuth obtained from the best-fitting kinematical parameters in Table 4. The red solid line, olive dash line, and blue dash-dot line denote the velocities of Sagittarius (Sgr), Local (Loc), and Perseus (Per) arms respectively. For each arm the Galactocentric distance is fixed at the sample mean $\langle R\rangle$ of all the sources resided in it: $\langle R\rangle = 6.0\,\mathrm{kpc}$, $7.7\,\mathrm{kpc}$, $9.4\,\mathrm{kpc}$ for Sagittarius, Local, and Perseus arms respectively. The upper panel shows the radial velocities $\bar{v}_R$ and the lower panel shows the azimuthal velocities $\bar{v}_\phi$.

values of p and R_0 are fixed at 0.2 and $7.63\,\mathrm{kpc}$ come from the estimation in Section 4.2. Table 4 lists the best-fitting parameters derived from different arms. Figure 5 presents the modeled rotation velocities as functions of azimuths for each arm.

It is clear that the rotation of each single arm deviates from a circular one and there are notable discrepancies among the rotation properties of different arms. The rotation ellipticity of the Sagittarius arm is $\gtrsim 0.02$ smaller than that of the Local and the Perseus, and the azimuth of the major axis of the Sagittarius's orbit is also $\gtrsim 10^\circ$ smaller than those of another two arms. Although the Local and the Perseus arms share similar rotation shapes, it is worth noting that the velocity dispersion of sources resided in the Perseus arm is much larger than in other two arms. The total velocity dispersion derived from the Perseus sources is approximately $10\,\mathrm{km\,s^{-1}}$ larger than that from the bluest stars in the *Hipparcos* catalogue (Dehnen&Binney 1998; Aumer&Binney 2009). Such significant peculiar motions in the Perseus arm could attribute to several causes. First, the heating process in the Perseus arm could be more violent than in other two arms, but there is no evidence that the Perseus arm is obviously warmer than others. Second, the large peculiar motions of Perseus sources could attribute to the probable interaction between the outer disk and the halo (Normandeau et al. 1996; Levine et al. 2006), but it is doubtful whether the halo could act significantly on the new-born stars. Third, the random motions of stars in the Perseus arm might not satisfy the Gauss' law. For the simplest case we adopt an isotropous Gaussian distribution for the random component of stellar velocities in all the arms, but the Gaussian distribution may have its limitations when describing the kinematics of the Perseus arm and there could be some un-modeled motions for the Perseus stars. Theoretically, a higher-order rotation model with more parameters could describe the stellar velocities in more detail, but the reliability of the constrained parameters in a more complex model undoubtedly depends on the sample completeness. The spiral arm is one of the dominating structures in the Galactic disk, and masers are good tracers of arm kinematics. More homogenous spacial distribution of observed masers will help us construct a detailed kinematical model for a spiral arm.

In this work we investigate the kinematical non-axisymmetry in the $(R,\,\phi)$-plane under an assumption that the equipotential surfaces of the Galaxy's potential are approximately elliptical. By exploiting

the maser data, a weak potential ellipticity of $\epsilon_0 \sim 0.09$ is detected. It is worth noting that there still exists some unknowns in stellar motions. On the one hand, regional distortions such as the distortion caused by Galactic warp or spiral waves (Miyamoto & Zhu 1998; Bobylev 2010; Bobylev&Bajkova 2015a) could increase the complexity of the stellar velocity field. On the other hand, the motion of masers suggests a larger ellipticity than that of later-type thin-disk objects (e.g. open clusters and Cepheids). More complete data of tracers will help us to explore the Galactic kinematics in different scales.

6 SUMMARY

The Milky Way's rotation can be distorted into an elliptical one by the non-axisymmetric potential of the Galaxy. In this work we describe the Milky Way's rotation shape using a non-axisymmetric rotation model formulated by KT94. Employing and generalizing the ML method formulated by AL13, we exploit the data thoroughly and analyze the elliptical rotation of our home galaxy traced by the maser sources selected from Reid et al. (2014).

The power-law index of the radius-dependent non-axisymmetric part of the Galaxy's potential, p, is estimated to be ~ 0.20, coupled with a potential ellipticity ~ 0.09 at the Sun, and the minor axis of the elliptical potential (the major axis of the orbit) is found to be near the Sun with a displacement $\sim 32^\circ$. Based on the KT94 model, we deal with a kinematical calibration of the Galactocentric distance of the Sun. An estimated value of $7.63 \pm 0.34\,\mathrm{kpc}$ is obtained in the final solution.

Acknowledgements This work is funded by the National Natural Science Foundation of China (NSFC) under grant Nos. 11303018 and 11473013 and the Natural Science Foundation of Jiangsu Province under No. BK20130546. We wish to thank the anonymous referee for useful comments and suggestions which helped to improve the manuscript.

References

Aghajani, T., & Lindegren, L. 2013, A&A, 551, A9
Aumer, M., & Binney, J. J. 2009, MNRAS, 397, 1286
Binney, J. 1978, MNRAS, 183, 779
Blitz, L., & Spergel, D. N. 1991, ApJ, 370, 205
Bobylev, V. V. 2010, Astronomy Letters, 36, 634
Bobylev, V. V. 2013, Astronomy Letters, 39, 95
Bobylev, V. V., & Bajkova, A. T. 2015, MNRAS, 447, L50
Bobylev, V. V., & Bajkova, A. T. 2015, Astronomy Letters, 41, 473
Bobylev, V. V., & Bajkova, A. T. 2017, Astronomy Letters, 43, 159
Boehle, A., Ghez, A. M., Schödel, R., et al. 2016, ApJ, 830, 17
Bovy, J., Allende Prieto, C., Beers, T. C., et al. 2012, ApJ, 759, 131
Chemin, L., Renaud, F., & Soubiran, C. 2015, A&A, 578, A14
Dehnen, W., & Binney, J. J. 1998, MNRAS, 298, 387
de Vaucouleurs, G. 1970, The Spiral Structure of our Galaxy, 38, 18
Dwek, E., Arendt, R. G., Hauser, M. G., et al. 1995, ApJ, 445, 716
Elias, F., Alfaro, E. J., & Cabrera-Caño, J. 2006, AJ, 132, 1052
Gerhard, O. 2016, The General Assembly of Galaxy Halos: Structure, Origin and Evolution, 317, 266
Gillessen, S., Eisenhauer, F., Trippe, S., et al. 2009, ApJ, 692, 1075
Huang, Y., Liu, X.-W., Yuan, H.-B., et al. 2016, MNRAS, 463, 2623
Kuijken, K. 1996, IAU Colloq. 157: Barred Galaxies, 91, 504
Kuijken, K., & Tremaine, S. 1994, ApJ, 421, 178
Levine, E. S., Blitz, L., Heiles, C., & Weinberg, M. 2006, arXiv:astro-ph/0609554
Lindegren, L., Lammers, U., Bastian, U., et al. 2016, A&A, 595, A4
López-Corredoira, M. 2014, A&A, 563, A128

López-Corredoira, M., & González-Fernández, C. 2016, AJ, 151, 165
Matsunaga, N., Feast, M. W., Kawadu, T., et al. 2013, MNRAS, 429, 385
McMillan, P. J., & Binney, J. J. 2010, MNRAS, 402, 934
Metropolis, N., Rosenbluth, A. W., Rosenbluth, M. N., Teller, A. H., & Teller, E. 1953, J. Chemical Phys., 21, 1087
Metzger, M. R., Caldwell, J. A. R., & Schechter, P. L. 1998, AJ, 115, 635
Miyamoto, M., & Zhu, Z. 1998, AJ, 115, 14833
Normandeau, M., Taylor, A. R., & Dewdney, P. E. 1996, NATURE, 380, 687
Pietrukowicz, P., Kozłowski, S., Skowron, J., et al. 2015, ApJ, 811, 113
Reid, M. J. 2012, Cosmic Masers - from OH to H0, 287, 359
Reid, M. J., & Dame, T. M. 2016, ApJ, 832, 159
Reid, M. J., Menten, K. M., Brunthaler, A., et al. 2014, ApJ, 783, 130
Rojas-Niño, A., Martínez-Medina, L. A., Pichardo, B., & Valenzuela, O. 2015, ApJ, 805, 29
Schönrich, R. 2012, MNRAS, 427, 274
Schönrich, R., Binney, J., & Dehnen, W. 2010, MNRAS, 403, 1829
Sharma, S., Bland-Hawthorn, J., Binney, J., et al. 2014, ApJ, 793, 51
Shen, M., & Zhu, Z. 2007, Chin. J. Astron. Astrophys., 7, 120
Uemura, M., Ohashi, H., Hayakawa, T., et al. 2000, PASJ, 52, 143
Zhu, Z. 2006, Chin. J. Astron. Astrophys., 6, 363
Zhu, Z. 2008, Chin. J. Astron. Astrophys., 8, 96

APPENDIX

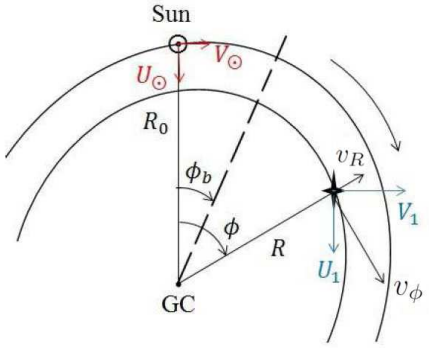

Fig. 6 Orbits of the Sun and the source in the Galactic plane for an assumed elliptical rotation. R_0 and R are the Galactocentric distances of the Sun and the source respectively. ϕ_b and ϕ are the azimuths of the major axis of the orbit and the source respectively. v_R and v_ϕ denote the velocities in the directions of increasing R and ϕ. U_1 and V_1 indicate the velocities relative to the Sun in the heliocentric Cartesian coordinate system in the directions u and v. $U_\odot$ and $V_\odot$ denote the solar peculiar motions.

In order to obtain the expressions of $\boldsymbol{v}$ and $\boldsymbol{D_v}$ in Sec. 3.2, we define heliocentric velocities U_1, V_1 and W_1 to be the velocities relative to the Sun in the three directions u, v and w in the heliocentric Cartesian coordinate system, respectively (see Fig. 6). In this case, $(U_1,\, V_1,\, W_1)$ can be calculated via

$$\begin{pmatrix} U_1 \\ V_1 \\ W_1 \end{pmatrix} = M_1 \begin{pmatrix} v_R \\ v_\phi \\ v_z \end{pmatrix} + \begin{pmatrix} +v_{R,(R=R_0,\,\phi=0^\circ)} \\ -v_{\phi,(R=R_0,\,\phi=0^\circ)} \\ 0 \end{pmatrix} - \boldsymbol{v}_\odot, \tag{13}$$

where M_1 is a 3×3 matrix

$$\boldsymbol{M}_1 = \begin{pmatrix} -\cos\phi & \sin\phi & 0 \\ \sin\phi & \cos\phi & 0 \\ 0 & 0 & 1 \end{pmatrix}. \tag{14}$$

that projects any vector from the Galactocentric cylindrical coordinate system to the heliocentric Cartesian coordinate system. Now the values of $\boldsymbol{v}$ can be obtained from $(U_1,\, V_1,\, W_1)$:

$$\boldsymbol{v} = M_2 \begin{pmatrix} U_1 \\ V_1 \\ W_1 \end{pmatrix}, \tag{15}$$

where M_2 is a 3×3 matrix:

$$\boldsymbol{M}_2 = \begin{pmatrix} -\sin l & \cos l & 0 \\ -\sin b\cos l & -\sin b\sin l & \cos b \\ \cos b\cos l & \cos b\sin l & \sin b \end{pmatrix}. \tag{16}$$

Finally the covariance of $\boldsymbol{D_v}$ resulted from the dispersion tensor $\boldsymbol{D}$ is in the following form:

$$\boldsymbol{D_v} = \boldsymbol{M_2 M_1 D M_1^T M_2^T}. \tag{17}$$